A&A 503, 765–770 (2009)
DOI: 10.1051/0004-6361/200912330

Astronomy & Astrophysics

Diffuse molecular gas at high redshift

Detection of CO molecules and the 2175 Å dust feature at $z = 1.64^{\star}$

P. Noterdaeme[1,3], C. Ledoux[2], R. Srianand[3], P. Petitjean[1], and S. Lopez[4]

[1] Université Paris 6, Institut d'Astrophysique de Paris, CNRS UMR 7095, 98bis bd Arago, 75014 Paris, France
e-mail: [noterdaeme;petitjean]@iap.fr
[2] European Southern Observatory, Alonso de Córdova 3107, Casilla 19001, Vitacura, Santiago 19, Chile
e-mail: cledoux@eso.org
[3] Inter-University Centre for Astronomy and Astrophysics, Post Bag 4, Ganeshkhind, 411 007 Pune, India
e-mail: [pasquiern;anand]@iucaa.ernet.in
[4] Departamento de Astronomía, Universidad de Chile, Casilla 36-D, Santiago, Chile
e-mail: slopez@das.uchile.cl

Received 15 April 2009 / Accepted 29 May 2009

ABSTRACT

We present the detection of carbon monoxide molecules (CO) at $z = 1.6408$ towards the quasar SDSS J160457.50+220300.5 using the Very Large Telescope Ultraviolet and Visual Echelle Spectrograph. We detected CO absorption in at least two components in the first six A−X bands and one d−X(5−0) interband system. This is the second detection of its kind along a quasar line of sight. The CO absorption profiles are well modelled by assuming rotational excitation of CO in the range $6 < T_{ex} < 16$ K, which is consistent with or higher than the temperature of the cosmic microwave background radiation at this redshift. We derive a total CO column density of $N(\mathrm{CO}) = 4 \times 10^{14}$ cm^{-2}. The measured column densities of S I, Mg I, Zn II, Fe II, and Si II indicate a dust depletion pattern typical of cold gas in the Galactic disc. The background quasar spectrum is significantly reddened ($u - K \sim 4.5$ mag) and exhibits a pronounced 2175 Å dust absorption feature at the redshift of the CO absorber. Using a control sample of ∼500 quasars, we find that the chance probability that this feature is spurious is ∼0.3%. We show that the spectral energy distribution (SED) of the quasar is well fitted by a QSO composite spectrum reddened with a Large Magellanic Cloud supershell extinction law at the redshift of the absorber. It is noticeable that this quasar is absent from the colour-selected SDSS quasar sample. This demonstrates that our current view of the Universe may be biased against dusty sightlines. These direct observations of carbonaceous molecules and dust open up the possibility of studying the physical conditions and chemistry of diffuse molecular gas in high redshift galaxies.

Key words. cosmology: observations – galaxies: ISM – quasars: absorption lines – quasars: individual: SDSS J160457.50+220300.5

1. Introduction

Quasar absorption lines provide a powerful tool for detecting and studying gaseous baryonic matter at all redshifts in a luminosity-unbiased way. Large column densities of neutral gas are detected through the damped Lyman-α absorption lines they imprint in the spectrum of background quasars. Because of the large neutral hydrogen column densities ($N(\mathrm{H\,I}) \gtrsim 10^{20}$ cm^{-2}), similar to those observed along Galactic lines of sight, and the presence of metals at different levels of chemical enrichment (e.g., Pettini et al. 1997; Prochaska & Wolfe 2002), it is believed that a large fraction of damped Lyman-α systems (DLAs) are located close to regions of star formation at high redshift (see, e.g., Wolfe et al. 2005, for a review on the subject).

The typical dust-to-gas ratio of DLAs, is generally less than one tenth of that observed in the local interstellar medium (ISM), and only a small fraction (∼10−15%) of DLAs show detectable amounts of molecular hydrogen (Ledoux et al. 2003; Noterdaeme et al. 2008a). Even in these cases, the molecular fractions are small compared to those measured in the Galactic ISM. It is therefore likely that most of the DLAs probe only diffuse neutral gas (Petitjean et al. 2000). In contrast, the detection of the cold ($T \sim 10$−100 K), dusty, and molecular gas, a fundamental ingredient of star-formation, has been elusive so far in absorption studies. The corresponding regions may have been missed because of the large extinction they are expected to produce. It could also be that molecular gas escapes detection because of its very small cross section (Zwaan & Prochaska 2006).

Gamma ray bursts (GRBs) are thought to be located in star-forming regions, and their associated absorptions are therefore more likely to represent the densest part of the ISM at high redshift. However, the physical state of the absorbing gas is likely to be influenced by the intense UV radiation field producing by the GRB itself (e.g., Vreeswijk et al. 2007). This could explain the absence of H_2 in the majority of GRB-DLAs (Tumlinson et al. 2007). However, only a handful of GRB-DLAs have been studied so far and existing data are still consistent with the statistics of H_2 detections in intervening QSO-DLA samples (Ledoux et al. 2009, submitted). When molecules are seen (Prochaska et al. 2009), their excitation is observed to be high, indicating strong UV pumping from the GRB afterglow.

We initiated a programme to search for cold gas along QSO lines of sight. The enormous number of quasar spectra available in the Sloan Digital Sky Survey (SDSS) and the faint magnitude

⋆ Based on observations carried out with the Ultraviolet and Visual Echelle Spectrograph, mounted on the ESO Very Large Telescope, under Prgm. ID. 081.A-0334(B).

limit achieved by the survey allow us to identify absorption systems with unique characteristics. In particular, the systems can be selected on the basis of the presence of C I, which should correspond predominantly to cold neutral gas. We searched for strong (W_r(C Iλ1656) $\sim$ 0.5 Å) C I absorbers at $z \sim 1.5-3$ along the line of sight of ~40 000 QSOs from the SDSS Data Release 7.

The selection leads to the first detection of carbon monoxide (CO) absorption lines at $z \sim 2.4$ (Srianand et al. 2008b). Similarly, selection of strong Mg II systems at intermediate redshift lead to the detection of the 2175 Å feature and 21-cm absorption in two $z \sim 1.3$ Mg II systems (Srianand et al. 2008a). Until now, direct signatures of dust at $z > 0$, such as the UV bump or diffuse interstellar bands (DIBs), have been reported in only a small number of cases (e.g., Motta et al. 2002; Wucknitz et al. 2003; Ellison et al. 2008; Liang & Li 2009).

In this paper, we present the simultaneous detection of carbon monoxide absorption lines and the 2175 Å dust feature in an intervening absorber at $z = 1.64$ towards SDSS J160457+220300. We present high spectral resolution observations in Sect. 2, the metal content of the system in Sect. 3, and the analysis of molecular lines in Sect. 4. We discuss the extinction and presence of a UV bump in Sect. 5. We finally present our conclusions in Sect. 6.

2. Observations

The quasar SDSS J160457.50+220300.5 ($z_{em} = 1.98$) was observed with the Ultraviolet and Visual Echelle Spectrograph (UVES; Dekker et al. 2000) in visitor mode on June 28–30, 2008. The total exposure time on source was 29 400 s. Both UVES spectrographic arms were used simultaneously, taking advantage of a dichroic setting with central wavelengths of 390 nm in the blue and 564 nm in the red. The resultant wavelength coverage was 329–451 nm and 462–665 nm with a gap between 559 and 568 nm corresponding to the physical gap between the two red CCDs. The CCD pixels were binned 2 × 2 and the slit width adjusted to 1″ to match the ambient seeing conditions. This yielded a resolving power of $R = 47\,500$ in the blue and $R = 45\,000$ in the red as measured from the Th-Ar lines of the calibration lamp. The data were reduced using the MIDAS-based UVES pipeline v 2.9.7, which performs an accurate tracking of the object while subtracting the sky spectrum at the same time. Cosmic-ray impacts and CCD defects were rejected iteratively. Wavelengths were rebinned to the vacuum-heliocentric rest frame and individual exposures were coadded using sliding windows and weighting the signal by the signal-to-noise ratio in each pixel. We analysed the spectrum using standard Voigt-profile fitting techniques. Oscillator strengths and wavelengths of CO absorption lines were taken from Morton & Noreau (1994) with updated values from Eidelsberg & Rostas (2003) for the interband systems. Heavy element abundances were measured relative to solar (Grevesse et al. 2007), as [X/H] $\equiv \log N(\mathrm{X})/N(\mathrm{H}) - \log (\mathrm{X/H})_\odot$ assuming that $N(\mathrm{H}) = N(\mathrm{H\,I})$. Throughout the paper, we refer to SDSS J160457.50+220300.5 as Q 1604+2203.

3. Metal content

Absorption lines from singly ionised metals (Fe II, Si II, and Zn II) as well as neutral species (S I, Mg I, and C I) are detected at about $z_{abs} = 1.6405$ over ~200 km s^{-1} (see Fig. 1).

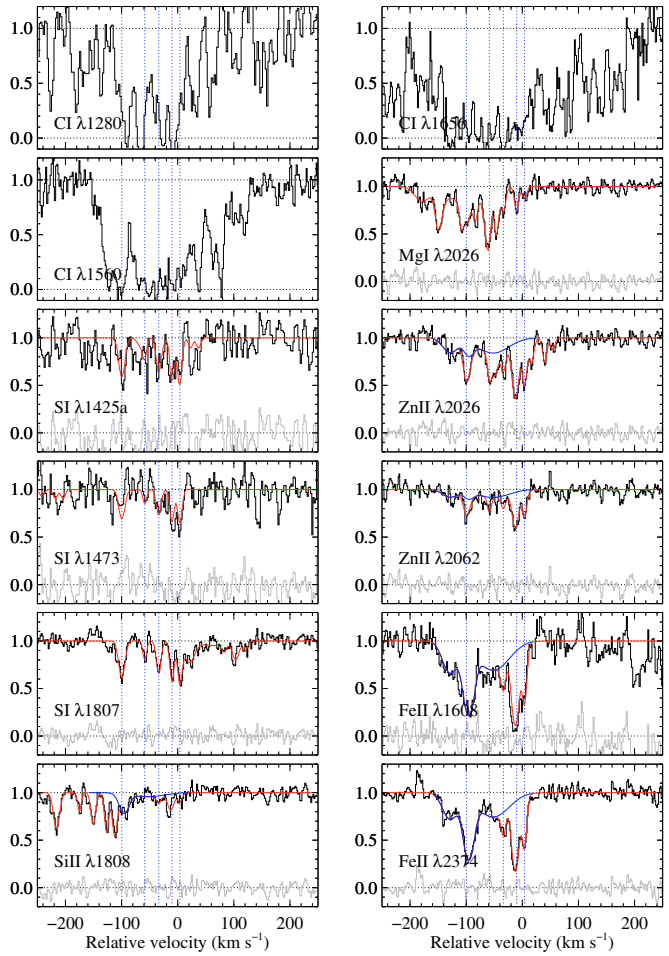

Fig. 1. Voigt-profile fit to neutral and singly ionised species. The origin of the velocity scale is taken at $z = 1.6408$. Vertical dotted lines indicate the position of narrow components ("N" in Table 1). The contribution from the broad components only ("B" in Table 1) is represented by the blue profile. The extremely strong C I lines, although not fitted, are also shown in *the top panels*. The C I λ1280 profile has been smoothed by 2 pixels for presentation purpose only.

The detected absorption lines of neutral species are exceptionally strong, where C I $\lambda\lambda$1560, 1656 is heavily saturated and S I clearly detected in several transitions. We note that S I is rarely seen in QSO absorbing systems (Quast et al. 2008; Srianand et al. 2008b). Fe I is not detected down to $\log N(\mathrm{Fe\,I}) = 11.4$ for each component (3σ upper limit). We performed simultaneous multi-component Voigt-profile fits with *fitlyman* (Fontana & Ballester 1995) to constrain redshifts, Doppler parameters b, and column densities, see Table 1. Five narrow components are required to fit the neutral species (S I and Mg I). The profiles of singly ionised species (Zn II, Si II and Fe II) require additional broad components.

While the narrow components can still be seen in the profiles of Zn II transitions, the presence of additional broad components introduces a degeneracy in the results in particular the relative column densities in the narrow and broad components. We associated the broad and narrow components somewhat artificially so that one could consider the sum of the column densities in the broad ($b > 10$ km s^{-1}) and narrow ($b < 10$ km s^{-1}) components to be representative of the column density in the six components listed in Table 1. Narrow components can be completely lost into the broad ones, as is the case for Fe II and Si II. *However, because lines are in the optically-thin regime, integrated column*

Table 1. Results of Voigt-profile fitting to detected lines at $z \sim 1.64$ in the spectrum of Q 1604+2203.

Comp.[a]	z	b (km s^{-1})	log $N(X)$ (cm^{-2})					
			Zn II	Fe II	Si II	Mg I	S I	CO
1B	1.63967	17.8 ± 0.8	12.31 ± 0.03	13.73 ± 0.02				
2N	1.63992	6.3 ± 0.4	12.34 ± 0.05			12.85 ± 0.04	13.18 ± 0.02	≤13.64
2B	1.63996	11.4 ± 0.3	12.09 ± 0.11	14.10 ± 0.01	14.72 ± 0.03			
3N	1.64028	2.8 ± 0.6	12.07 ± 0.04				12.64 ± 0.05	≤13.28
3B	1.64034	37.6 ± 1.4	12.67 ± 0.04	14.00 ± 0.02	14.52 ± 0.09			
4N	1.64080	4.5 ± 0.4	12.06 ± 0.05	13.29 ± 0.04	13.96 ± 0.13	12.73 ± 0.03	13.01 ± 0.02	≤13.80
5N	1.64069	6.8 ± 0.3	12.70 ± 0.03	14.08 ± 0.01	14.45 ± 0.05			
	1.64071	3.6 ± 0.4				12.66 ± 0.04	13.10 ± 0.02	14.24 ± 0.20
6N	1.64083	3.9 ± 0.3	12.42 ± 0.02	13.67 ± 0.02	14.02 ± 0.10	12.33 ± 0.07	13.13 ± 0.02	14.34 ± 0.10
Total			13.30 ± 0.02	14.67 ± 0.01	15.13 ± 0.03	13.28 ± 0.02	13.75 ± 0.01	14.59 ± 0.11 [b]

[a] Narrow components ($b < 10$ km s^{-1}) are indicated by "N" while "B" stands for broad component ($b > 10$ km s^{-1}); [b] total N(CO) measured from comp. 5 and 6 only. Undetected components (2N, 3N and 4N) could increase this value by up to 0.1 dex (see text).

densities will not depend upon the true number of components. The above decomposition shows that the coldest gas, as traced by the S I components, is found in clumps embedded in a more turbulent and probably warmer phase. This structure is natural (see e.g. Petitjean et al. 1992) and is usually observed in the H_2 phase of DLAs (Ledoux et al. 2002). The immediate consequence of this is that the depletion factor estimated from integrated column densities may not be a correct representation of the true depletion factors for individual components.

Using the integrated column densities (Table 1) and upper limits for different ions (log N(Ni II) < 13.2 and log N(Cr II) < 12.8 at 3σ c.l., for the whole profile), we find, [Fe/Zn] = −1.47, [Si/Zn] = −1.07, [Ni/Zn] < −1.5, and [Cr/Zn] < −1.3. This is consistent with the depletion pattern seen in the cold neutral medium of the Galactic ISM and that of the Large Magellanic Cloud (see Welty et al. 1999).

From the equivalent width of C I λ1280, which is the weakest C I line available, we derive log N(C I) > 15.3, in the linear regime limit. However, even this line is saturated, and filling the C I profiles with five components with the same parameters – Doppler parameters and redshifts – as the S I components gives log N(C I) > 16.0, which is still a lower limit. Therefore, this system has by far the highest column densities of C I and S I known in any QSO absorption system.

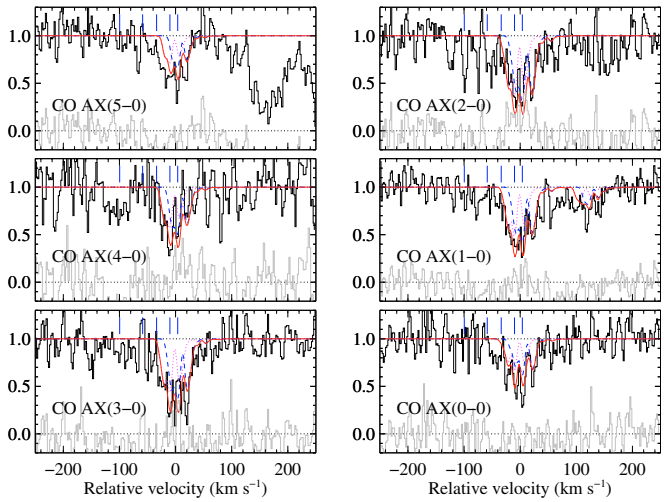

Fig. 2. Voigt profile fit to detected CO absorption lines. The origin of the velocity scale, is taken to be $z = 1.6408$. Additional absorption in the CO A−X (1−0) panel at $v \sim 150$ km s^{-1} is due to the d−X (5−0) inter band system. The contribution from individual components is shown at the position of the two reddest S I components (short vertical marks) by dotted and dashed profiles.

4. Carbon monoxide

Carbon monoxide absorption lines are detected in several A−X bands and the d−X (5−0) inter band system.

Following Burgh et al. (2007), we used the excitation temperature as an external parameter. We fitted the CO profile using a IDL code based on MPFIT (Markwardt 2009), which performs χ^2-minimisation by applying the Levenberg-Marquardt technique. Components associated with the reddest S I components, at $z = 1.64071$ and 1.64083, are clearly detected in the $J = 0$ and $J = 1$ rotational levels (see Fig. 2). The S/N ratio of the data is not high enough for an independent fit to be performed. In addition, lines from different rotational levels are blended. We therefore fixed the redshifts and Doppler parameters to those obtained from S I. We varied only the total CO column density for each of the two components, distributed among rotational levels up to $J = 3$, using a single excitation temperature T_{ex}.

If we assume that the excitation of CO is caused by the cosmic microwave background radiation alone, i.e., $T_{ex} = T_{CMBR}(z = 1.64)$, then the best-fit model is achieved with $\chi^2_\nu = 1.08$ for a total column density log N(CO) = 14.6. The model is superimposed on the observed spectrum in Fig. 2.

For low gas pressure (Srianand et al. 2008b) and in the absence of UV pumping, T_{ex} and T_{CMBR} are expected to be equal. Excitation by photon trapping becomes significant only when $N(CO) > 10^{16}$ cm^{-2} (Burgh et al. 2007). Unfortunately, unlike the case of the $z_{abs} = 2.42$ CO-bearing system towards SDSS J143912+111740, all observed neutral carbon lines are saturated and it is therefore impossible to estimate the gas pressure from the population of C I fine-structure levels. We fitted different models along a grid of excitation temperatures and Doppler parameters. A good fit ($\chi^2 \lesssim 1.2$) was achieved for a CO excitation temperature equal to or higher than the CMBR temperature and for $b > 0.4$ km s^{-1}. We inferred that $6 < T_{ex} < 16$ K at the 5σ confidence level.

The assumption of a single excitation temperature for all rotational levels may be too inaccurate. However, T_{0J} is generally found to be constant for $J \leq 3$ in diffuse molecular gas in the local Universe (Sheffer et al. 2008). Most of the optical depth of the CO profile can be attributed to absorption from $J = 0$ and $J = 1$. A two rotational level model provides the same results.

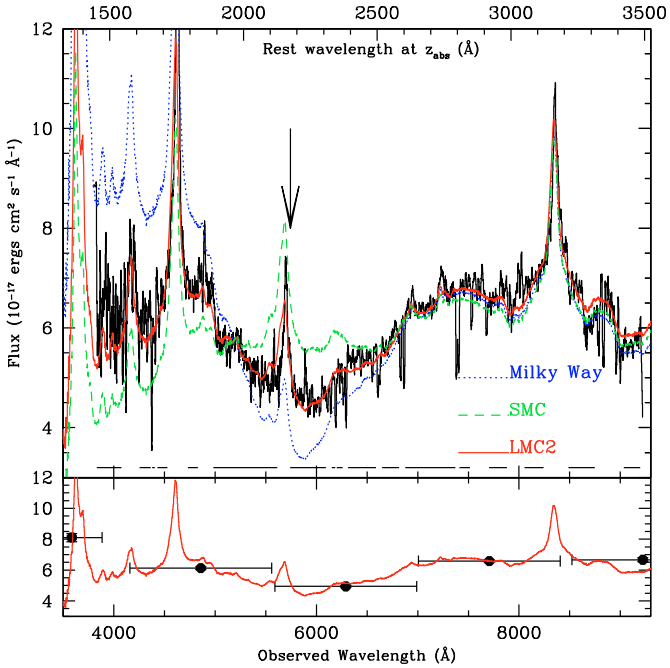

Fig. 3. SDSS spectrum of SDSS J160457+220300 fitted with the SDSS composite spectrum reddened by mean extinction curves from the Galaxy (dotted line), the LMC2 supershell (solid line) and the SMC (dashed line). The arrow indicates the position of the 2175 Å feature at $z_{abs} = 1.64$. The spectral regions used for χ^2 minimisation are marked by solid lines at the bottom of *the top panel*. The observed spectrum is boxcar smoothed by 10 pixels for presentation purpose. The best-fit model and the SDSS photometric points are shown in *the bottom panel*.

We checked that the total CO column density varies by less than 0.10 dex regardless of the b and T_{ex} values, as long as the condition $\chi^2 < 1.2$ is fulfilled. The decomposition of the profile in different components is however quite uncertain.

In the three bluest S I components, CO may also be present although not detected directly at the 3σ level. Because these components are far enough away from the two detected CO components, they have little influence on the excitation temperature. However, they could contribute to increase the overall CO column density (over the range $v = -150$ to $+50$ km s^{-1}) by 0.1 dex.

From the lower limit to N(C I), we infer that N(CO)/N(C I) $\leq$ 0.05, which is typical of that measured in the diffuse molecular medium (Federman et al. 1980).

5. Dust and 2175 Å UV bump

The presence of dust grains influences the physical state of the gas by means of photo-electric heating, UV shielding, and the formation of molecules on the surface of grains. It can be deduced from the depletion pattern of different elements (see Sect. 3) and/or from the reddening of the background QSO.

The spectral energy distribution (SED) of Q 1604+2203 is very red with $u - K \sim 4.5$ mag. We note that this value is only indicative since u (SDSS) and K (2MASS) magnitudes were measured with 4 years interval and the true $u - K$ value could be different because of quasar optical variability. The flux-calibrated SDSS spectrum of Q 1604+2203 is visibly affected by reddening and also exhibits clear curvature around 2175 Å in the rest frame of the $z = 1.64$ absorbing system (see Fig. 3). We investigate the possibility that the red colour of the quasar is due to the presence of dust in the CO-bearing system.

Table 2. Results of fitting the SED of Q 1604+2203 with different extinction curves.

Extinction law	R_V	$E(B-V)$	χ^2_ν
MW	3.1	0.26 ± 0.01	3.0
LMC	3.4	0.24 ± 0.02	1.6
LMC2	2.7	0.27 ± 0.02	1.2
SMC	2.7	0.16 ± 0.02	2.1

We performed a χ^2-minimisation between the data and a SDSS composite spectrum (Vanden Berk et al. 2001) reddened by different types of extinction curves, namely that from the Small Magellanic Cloud (SMC), Large Magellanic Cloud Supershell (LMC2), Large Magellanic cloud (LMC) and the Galaxy (MW) (Gordon et al. 2003). The strength of the 2175 Å bump differs significantly from one extinction curve to another: while the UV bump is absent in the SMC extinction curve, it has its strongest value in the MW and LMC extinction curves. In addition, the SMC extinction curve has a large UV extinction at $\lambda < 2000$ Å, compared to the LMC and MW extinction curves. The average extinction curve of the LMC supershell (LMC2), which is part of the 30 Dor star-forming region, has a bump strength and a UV extinction in-between the two extremes.

Results of our best-fit models using different extinction curves are presented in Table 2. A detailed description of the procedure can be found in Srianand et al. (2008a). The lowest reduced χ^2 value is reached for the LMC2 supershell dust extinction curve with $E(B-V) = 0.27 \pm 0.02$ for $R_V = 2.7$.

For a sample of SDSS spectra, we performed a test to exclude the possibility that a peculiar intrinsic spectral shape is mistaken for a 2175 Å bump (Pitman et al. 2000). Our control sample consists of all 529 SDSS quasars with emission redshift within $\Delta z = \pm 0.01$ of that of Q 1604+2203 ($z_{em} = 1.979$). The distribution of S/N ratios of the spectra[1] is shown in the upper right panel of Fig. 4. We fitted all quasar spectra using the SDSS composite spectrum reddened by a SMC extinction curve shifted to $z_{abs} = 1.64$, *which does not exhibit any UV bump.* Using χ^2 minimisation, we estimated, for each quasar, $E(B-V)$ and the strength of a possible 2175 Å feature. The latter is calculated to be the integrated flux difference between the fitted composite spectrum and the observed QSO spectrum in the region where the 2175 Å bump is redshifted (i.e., over the observed wavelength range, $5203 \leq \lambda(\text{Å}) \leq 6571$). We parametrised this quantity by $\Delta_f = \left\langle F_{QSO}/F_{composite} - 1 \right\rangle$. A plot of Δ_f versus $E(B-V)$ together with the distributions of the two parameters is presented in Fig. 4. The positions of Q 1604+2203 in these graphs are indicated by arrows.

As expected, QSOs with low signal-to-noise ratio spectra (i.e., $S/N \leq 10$, open squares in the plots) are responsible for most of the scatter and a tail in the Δ_f distribution. Therefore, greater confidence is achieved when selecting only high signal-to-noise spectra (i.e., $S/N \geq 10$). Note Q 1604+2203 has $S/N = 14.7$. From the scatter plot of $E(B-V)$ versus Δ_f, it can be seen that the maximum deviation on both axis is seen for Q 1604+2203. The probability of measuring $E(B-V) > 0.15$ is as low as 0.7% when we consider only the high S/N (>10) spectra. This corresponds to a 4.7σ significance if we approximate the $E(B-V)$ distribution for spectra of $S/N > 10$ by a Gaussian function of mean zero and standard deviation 0.035.

[1] Median signal-to-noise ratio in the i-band (SN_I) provided by SDSS together with the 1D spectra (spSpec*.fit).

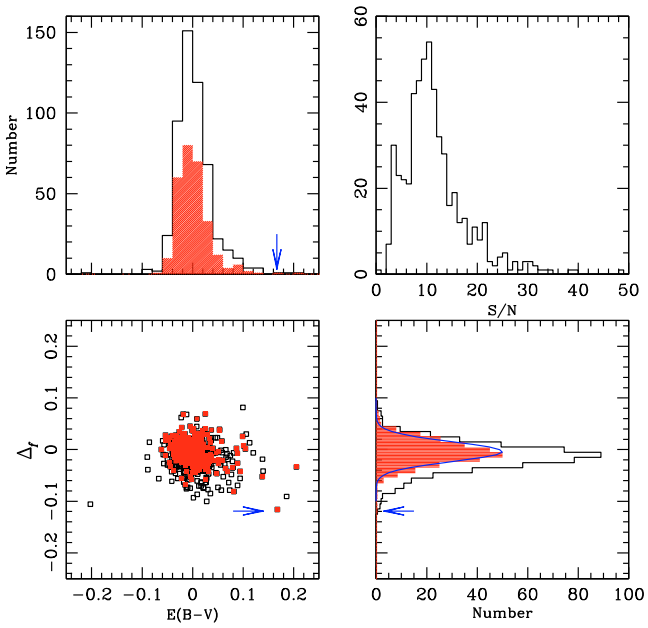

Fig. 4. Distributions of reddening ($E(B-V)$) and strength of the 2175 Å bump (Δ_f) for the control sample of 529 quasars with $z_{em} \in [1.969, 1.989]$. The arrows mark the position of SDSS J160457+220300 in the different panels. Red filled squares and histograms indicate measurements in spectra with signal-to-noise ratios larger than 10. *The top right panel* shows the distribution of the signal-to-noise ratios.

There is only one quasar (SDSS J131903+431034) in the high S/N control sample with a large $E(B-V)$ in addition to Q 1604+2203. Interestingly, two strong Mg II systems are present in the spectrum of this QSO. Selecting quasars with red colours could therefore provide a direct way for searching for dusty intervening absorbers. Concerning the 2175 Å absorption itself, only one quasar (the one presented here) has $\Delta_f < -0.10$. The corresponding probability is thus 0.4%. The mean Δ_f is zero with a 1σ dispersion of 0.035. So if we assume that the Δf distribution for spectra with $S/N > 10$ is well modelled by a Gaussian distribution, the confidence level on the UV bump detection is 4.3σ. The joint probability of measuring $E(B-V) > 0.15$ and $\Delta_f < -0.10$ by pure chance coincidence is 0.3%. In short, the exercise presented above excludes the possibility of the 2175 Å structure being spurious at a very high confidence level.

It is possible to estimate $N(\mathrm{H\,I})$ from the reddening of the quasar, by assuming the average LMC supershell relation between the column density of neutral gas and the extinction (Gordon et al. 2003)

$$\frac{N(\mathrm{H\,I})}{A_V} \simeq (6.97 \pm 0.67) \times 10^{21}\ \mathrm{cm^{-2}\ mag^{-1}}, \quad (1)$$

where $A_V = R_V \times E(B-V)$, and $R_V = 2.76 \pm 0.09$ is the average value for the LMC2 supershell. We then infer that $N(\mathrm{H\,I}) \sim 5 \times 10^{21}$ cm^{-2}. We can derive a lower limit to $N(\mathrm{H\,I})$ using the largest value of $A_V/N(\mathrm{H\,I}) = 3.76 \times 10^{-22}$ mag/(H cm^{-2}) measured in the LMC2 by Dobashi et al. (2008), $N(\mathrm{H\,I}) > 2 \times 10^{21}$ cm^{-2}. We note that $E(B-V)$ values obtained with different extinction laws (Table 2) and their corresponding $A_V/N(\mathrm{H\,I})$ ratios, provide very similar results. It would be very interesting to obtain a direct measurement of $N(\mathrm{H\,I})$. However, the faintness of the quasar in the blue ensures that any measurement with UVES would be difficult.

6. Discussion

We have reported the detection of diffuse molecular gas at $z_{abs} = 1.64$ towards the QSO SDSS J160457.50+220300.5, following careful selection of the target among several thousand quasars from the SDSS.

High spectral resolution observations with the UVES reveal the presence of CO molecules in the absorbing gas. This is only the second such detection in an intervening DLA along a quasar line of sight. By modelling the CO absorption with a multiple Voigt-profile pattern, we have measured the CO column density to be $N(\mathrm{CO}) = 4 \times 10^{14}$ cm^{-2} and an excitation temperature of the molecules, $6 < T_{ex} < 16$ K at the 5σ c.l., consistent with or higher than the expected temperature of the CMBR, $T_{CMBR} = 7.2$ K at $z = 1.64$.

The observed SED of the quasar is well reproduced if dust reddening happens in the CO absorber with an extinction law corresponding to that observed in the LMC2 supershell including a 2175 Å UV bump. We derive significant reddening ($E(B-V) = 0.27$) and a depletion pattern similar to that seen in the diffuse molecular medium of the local interstellar medium.

Statistical studies have shown that DLAs, as a general population, do not produce significant reddening of the light from the background quasar, $E(B-V)$ being less than about 0.04 mag (Murphy & Liske 2004; Ellison et al. 2005). Vladilo et al. (2008) found a low mean extinction-to-gas ratio in DLAs $A_V/N(\mathrm{H\,I}) \sim 2\text{–}4 \times 10^{-23}$ mag cm^2 in the SDSS-DR5. In addition, while strong Ca II absorbers seem to contain larger amounts of dust, they still produce only moderate reddening of the background quasar ($E(B-V) \sim 0.1$; Wild et al. 2006). Significant reddening, similar to that derived here, has only been found to date for a few individual absorption systems at low and intermediate redshift. Junkkarinen et al. (2004) report $E(B-V) = 0.23$ for the peculiar absorber at $z_{abs} = 0.52$ towards AO 0235+164, which also exhibits a 2175 Å bump at the same redshift. $E(B-V) = 0.16$, but no UV bump has been found toward SDSS J1323−0021 in a high-metallicity sub-DLA at $z_{abs} = 0.72$ (Khare et al. 2004). Ellison et al. (2008) detected DIBs in a Ca II absorber at $z_{abs} = 0.16$ towards a reddened quasar with $E(B-V) = 0.23$. Srianand et al. (2008a) measured an $E(B-V)$ of about 0.3 and detected 2175 Å dust features in two $z \sim 1.3$ 21-cm absorbers.

It is interesting to note that the depletion pattern of the present system is similar to what has been observed in the $z_{abs} = 2.418$ DLA towards SDSS J143912+111740 where CO is also detected (Srianand et al. 2008b). The present system has CO and S I column densities six times larger than in the previous system, whereas the integrated column densities of Zn II, Si II, and Fe II are only twice as large (Noterdaeme et al. 2008b).

The quasar Q 1604+2203 is outside the quasar locus used by SDSS to select spectroscopic targets (Richards et al. 2002) because of its red colours. More specifically, the object was flagged as `TARGET_QSO_REJECT` on the basis of its colours, and serendipitously assigned an excess spectroscopic fibre left over after the main samples of galaxies, LRGs, and quasars had been tiled (Stoughton et al. 2002). We also note that this object is absent from the photometric catalogue of $\sim 10^6$ quasars in SDSS-DR6 (Richards et al. 2009). Similarly, the dusty absorber at $z = 1.3$ towards SDSS J085244+343540 (Srianand et al. 2008a), is also absent from this catalogue and selected as a SDSS spectroscopic target only because the background quasar is radio-loud. This supports the proposal that lines of sight towards colour-selected quasars are probably biased against the detection of the most relevant component of the interstellar medium, i.e., the diffuse molecular and translucent lines of sight.

It has been four decades since the first detections of the 2175 Å extinction feature in the spectra of hot stars (Stecher 1965). While it now seems clear that the presence of this bump is related to that of small dust grains, the composition of these grains remains debated. Theoretical and experimental studies have shown that carbon-rich organic grains and polycyclic aromatic hydrocarbons (PAHs) are the most likely carriers of the 2175 Å feature. Amorphous silicates, abundant in interplanetary dust particles, could also contribute to the bump (Bradley et al. 2005).

The absence of UV bump in SMC lines-of-sight and in most starburst galaxies led Gordon et al. (1997) to propose a trend in dust properties with star formation intensity. The UV bump carriers could be extremely sensitive to both the local chemical enrichment and the energy input into the gas (e.g., Whittet 2003; Gordon et al. 2003; Noll et al. 2007). This is supported by theoretical work in the case of PAH clusters (Rapacioli et al. 2006) and could explain why such a feature is absent in the environment of most gamma-ray bursts (see however Elíasdóttir et al. 2009; Liang & Li 2009) and Lyman break galaxies (Vijh et al. 2003), and only present when the dust is shielded enough from the incident UV radiation.

An efficient shielding of the UV radiation field and high metal abundances may thus be necessary for the presence of small carbon-rich grains (see also Sloan et al. 2008). These are the ideal conditions for forming molecules efficiently (e.g., Ledoux et al. 2003; Srianand et al. 2005; Petitjean et al. 2006; Noterdaeme et al. 2008a), and in particular CO.

The observations reported here demonstrate that carbonaceous molecules and grains already exist at $z = 1.64$. This provides exciting prospects for studying organic chemistry at high redshift.

Acknowledgements. We are grateful to the anonymous referee for insightful comments and suggestions and to Claire Halliday for language editing. P.N. acknowledges support from the french Ministry of Foreign and European Affairs. S.L. was supported by FONDECYT grant No. 1060823. We acknowledge the use of the Sloan Digital Sky Survey database (http://www.sdss.org).

References

Bradley, J., Dai, Z. R., Erni, R., et al. 2005, Science, 307, 244
Burgh, E. B., France, K., & McCandliss, S. R. 2007, ApJ, 658, 446
Dekker, H., D'Odorico, S., Kaufer, A., Delabre, B., & Kotzlowski, H. 2000, in Optical and IR Telescope Instrumentation and Detectors, ed. M. Iye, & A. F. Moorwood, Proc. SPIE, 4008, 534
Dobashi, K., Bernard, J.-P., Hughes, A., et al. 2008, A&A, 484, 205
Eidelsberg, M., & Rostas, F. 2003, ApJS, 145, 89
Elíasdóttir, Á., Fynbo, J. P. U., Hjorth, J., et al. 2009, ApJ, 697, 1725
Ellison, S. L., Hall, P. B., & Lira, P. 2005, AJ, 130, 1345
Ellison, S. L., York, B. A., Murphy, M. T., et al. 2008, MNRAS, 383, L30
Federman, S. R., Glassgold, A. E., Jenkins, E. B., & Shaya, E. J. 1980, ApJ, 242, 545
Fontana, A., & Ballester, P. 1995, The Messenger, 80, 37
Gordon, K. D., Calzetti, D., & Witt, A. N. 1997, ApJ, 487, 625
Gordon, K. D., Clayton, G. C., Misselt, K. A., Landolt, A. U., & Wolff, M. J. 2003, ApJ, 594, 279
Grevesse, N., Asplund, M., & Sauval, A. J. 2007, Space Sci. Rev., 130, 105
Junkkarinen, V. T., Cohen, R. D., Beaver, E. A., et al. 2004, ApJ, 614, 658
Khare, P., Kulkarni, V. P., Lauroesch, J. T., et al. 2004, ApJ, 616, 86
Ledoux, C., Srianand, R., & Petitjean, P. 2002, A&A, 392, 781
Ledoux, C., Petitjean, P., & Srianand, R. 2003, MNRAS, 346, 209
Liang, S. L., & Li, A. 2009, ApJ, 690, L56
Markwardt, C. B. 2009 [arXiv:0902.2850]
Morton, D. C., & Noreau, L. 1994, ApJS, 95, 301
Motta, V., Mediavilla, E., Muñoz, J. A., et al. 2002, ApJ, 574, 719
Murphy, M. T., & Liske, J. 2004, MNRAS, 354, L31
Noll, S., Pierini, D., Pannella, M., & Savaglio, S. 2007, A&A, 472, 455
Noterdaeme, P., Ledoux, C., Petitjean, P., & Srianand, R. 2008a, A&A, 481, 327
Noterdaeme, P., Petitjean, P., Ledoux, C., Srianand, R., & Ivanchik, A. 2008b, A&A, 491, 397
Petitjean, P., Bergeron, J., & Puget, J. L. 1992, A&A, 265, 375
Petitjean, P., Srianand, R., & Ledoux, C. 2000, A&A, 364, L26
Petitjean, P., Ledoux, C., Noterdaeme, P., & Srianand, R. 2006, A&A, 456, L9
Pettini, M., Smith, L. J., King, D. L., & Hunstead, R. W. 1997, ApJ, 486, 665
Pitman, K. M., Clayton, G. C., & Gordon, K. D. 2000, PASP, 112, 537
Prochaska, J. X., & Wolfe, A. M. 2002, ApJ, 566, 68
Prochaska, J. X., Sheffer, Y., Perley, D. A., et al. 2009, ApJ, 691, L27
Quast, R., Reimers, D., & Baade, R. 2008, A&A, 477, 443
Rapacioli, M., Calvo, F., Joblin, C., et al. 2006, A&A, 460, 519
Richards, G. T., Fan, X., Newberg, H. J., et al. 2002, AJ, 123, 2945
Richards, G. T., Myers, A. D., Gray, A. G., et al. 2009, ApJS, 180, 67
Sheffer, Y., Rogers, M., Federman, S. R., et al. 2008, ApJ, 687, 1075
Sloan, G. C., Kraemer, K. E., Wood, P. R., et al. 2008, ApJ, 686, 1056
Srianand, R., Petitjean, P., Ledoux, C., Ferland, G., & Shaw, G. 2005, MNRAS, 362, 549
Srianand, R., Gupta, N., Petitjean, P., Noterdaeme, P., & Saikia, D. J. 2008a, MNRAS, 391, L69
Srianand, R., Noterdaeme, P., Ledoux, C., & Petitjean, P. 2008b, A&A, 482, L39
Stecher, T. P. 1965, ApJ, 142, 1683
Stoughton, C., Lupton, R. H., Bernardi, M., et al. 2002, AJ, 123, 485
Tumlinson, J., Prochaska, J. X., Chen, H.-W., Dessauges-Zavadsky, M., & Bloom, J. S. 2007, ApJ, 668, 667
Vanden Berk, D. E., Richards, G. T., Bauer, A., et al. 2001, AJ, 122, 549
Vijh, U. P., Witt, A. N., & Gordon, K. D. 2003, ApJ, 587, 533
Vladilo, G., Prochaska, J. X., & Wolfe, A. M. 2008, A&A, 478, 701
Vreeswijk, P. M., Ledoux, C., Smette, A., et al. 2007, A&A, 468, 83
Welty, D. E., Frisch, P. C., Sonneborn, G., & York, D. G. 1999, ApJ, 512, 636
Whittet, D. C. B. 2003, Dust in the galactic environment
Wild, V., Hewett, P. C., & Pettini, M. 2006, MNRAS, 367, 211
Wolfe, A. M., Gawiser, E., & Prochaska, J. X. 2005, ARA&A, 43, 861
Wucknitz, O., Wisotzki, L., Lopez, S., & Gregg, M. D. 2003, A&A, 405, 445
Zwaan, M. A., & Prochaska, J. X. 2006, ApJ, 643, 675